ELSEVIER

Materials Science and Engineering A271 (1999) 70–78

MATERIALS SCIENCE & ENGINEERING A

www.elsevier.com/locate/msea

Model experiment on a protrusion method for measurement of interface shear sliding stress in fiber-reinforced composite

Y. Kagawa [a,*], C.-H. Hsueh [b]

[a] *Institute of Industrial Science, The University of Tokyo 7-22-1, Roppongi, Minato-ku, Tokyo 106-8558, Japan*
[b] *Oak Ridge National Laboratory, P.O. Box 2008, Oak Ridge, TN 37831-6069, USA*

Received 9 March 1999

Abstract

Interface debonding, sliding and protrusion behavior in tungsten fiber-reinforced epoxy matrix model composite under 'protrusion test' have been studied. Interface shear-sliding resistance of the composite is obtained from three routes: (i) applied stress-sliding length relation; (ii) applied maximum stress-protruded fiber length at loading; and (iii) applied maximum stress and protruded fiber length after unloading. The shear sliding stress is obtained applying a constant shear stress analysis. It is found that interface debonding proceeds spontaneously with the increase of applied stress from the surface at a soft metal side and one unit of debonding is about twice the fiber radius. The constant interface shear stress approach could explain applied stress-interface sliding length relation below a maximum critical applied stress. The shear sliding stresses obtained from the three routes agree and the agreement demonstrated possibility of obtaining the constant shear frictional stress using a protruded fiber length after complete unloading. However, care should be taken to eliminate Poisson's effect; i.e. a maximum applied stress exists for a given composite and experimental condition. © 1999 Elsevier Science S.A. All rights reserved.

Keywords: Composite material; Shear sliding stress; Fiber protrusion behavior

1. Introduction

Various continuous fiber-reinforced composites are being considered for structural applications because of their unique properties, which are difficult to be achieved by monolithic materials. Researches demonstrated importance of interface shear mechanical properties on mechanical properties of composites. Thus, recently it has been commonly agreed that the measurement of interface mechanical properties is an important subject of research in the field of composites. To measure interface mechanical properties of fiber-reinforced composites, fiber pushin tests [1–5] and fiber pushout tests [5–10] have been widely applied. These methods are relatively simple and the tests provide interface shear debonding and sliding resistance of the composite without preparing of a special specimen for the test. Researches, both experimentally and theoretically, in these tests have been reported and they have been applied for the measurement of interface shear mechanical properties.

Recently, a more simple technique named 'protrusion test' [11,12] or 'slice compression test' [13,14] has been developed. The method is simple and has a potential for evaluation of interface shear properties for the composites with $E_f > E_m$ (E_f and E_m are Young's moduli of fiber and matrix, respectively). The technique was successfully applied for the measurement of interface shear sliding resistance in SiC(Nicalon ™) fiber-reinforced LAS matrix composite [11,12] and SiC(SCS-6) fiber-reinforced glass matrix composites [13,14]. The technique was also applied for the measurement of high temperature interface shear sliding stress in SiC(-Nicalon™) fiber-reinforced LAS matrix composite [12]. Theoretical analyses in various levels of assumptions on the test were reported [11,12,15,16].

* Corresponding author. Tel.: +81-3-3402-6231; fax: +81-3-3402-6350.

E-mail address: kagawa@iis.u-tokyo.ac.jp (Y. Kagawa)

0921-5093/99/$ - see front matter © 1999 Elsevier Science S.A. All rights reserved.
PII: S0921-5093(99)00166-5

Table 1
Properties of fiber and matrix.

	Young's Modulus (GPa)	Poisson's ratio	Coefficient of thermal expansion ($\times 10^{-6}$ K^{-1})
Tungsten fiber	380	0.17	4.6
Epoxy matrix	3	0.37	60

However, interface sliding and protrusion process of fiber from matrix during and after a protrusion test are not well examined experimentally. For example, the interface shear sliding stress is usually derived from a fiber protruded length using the shear-lag analysis which assumes a constant interface shear frictional stress. Thus the interface properties are determined from properties of fiber, matrix, fiber volume fraction and experimentally obtained fiber protruding length. The fiber protruded behavior involves forward and reverse interface sliding behavior during the loading and unloading process [11,12,15,16]. The theoretical analysis suggests importance of Poisson's effect as well as thermal stress on shear interfacial stress [15,16]. Although, the protrusion behavior is affected by various factors, no detailed report on the experimental evidence to prove various effects. The present study is aimed at investigating the detailed observation of an interface sliding process and fiber protrusion length. The interface shear sliding stress is obtained from three different routes which use experimentally obtainable values. Comparisons between the obtained interface shear sliding stresses from three different approaches are discussed.

2. Experimental procedure

2.1. Composite material

A 500 μm in diameter single tungsten (W) fiber-reinforced epoxy matrix model composite was used. Properties of the fiber and matrix are listed in Table 1 [17–19]. The ratio of Young's modulus between the fiber and matrix, E_f/E_m, is $\cong 127$. The matrix epoxy employed was clear grade epoxy resin (Epicote 828, Yuka-shell, Tokyo, Japan). The resin was cured using 46 wt.% of curing agent (MH-700, Shin-nihonrika, Tokyo, Japan) and 0.13 wt.% of accelerator (DBU, Sum-Apro, Tokyo, Japan). The above three base components were mixed in ambient air; poured into a Tefion®-coated tray (typically $100 \times 150 \times 30$ mm in depth) in which single W fiber was placed. Then, the tray was put under a vacuum of 10^{-2} Pa for 20 min, to expel dissolved air introduced during the mixing process. After this, the material was cured at 373 K for 2 h and post cured for 5 h at 383 K and cooled to room temperature (297 K).

After the fabrication of composite, the composite specimen was cut and polished by conventional metallurgical procedures. The shape and dimensions of specimen are shown in, Fig. 1. The nominal fiber volume fraction in the composite was ≈ 0.008.

The surfaces of the specimen were polished up to 0.1 μm diamond paste finish. The maximum compressive load applied during the polishing process was less than 50 N (≈ 2 MPa). However, most of the interfaces near the polished surfaces were debonded during the preparation process. The initial debonding length, l_d^0, was easy to detect by the change of light reflection at the interface, and the debond length ranged from 0.5 to 3 mm.

2.2. Test procedure

Before the test, the specimen was fully dried in air to remove the retained water in the specimen. This process was important to reduce the effect of water on shear sliding stress [20]. Fig. 2 shows a schematic drawing of the loading assembly. The composite specimen was sandwiched between a soft metal plate (thickness: 2 mm, fully annealed A1100, Young's modulus: $E = 60$ GPa, yield stress: ≈ 9 MPa) and a hard plate (thickness: 5 mm, sintered α-SiC, $E = 480$ GPa). The fiber axis was located perpendicular to the flat plane of these plates, i.e. parallel to the loading axis. A compressive load was applied to the sandwiched composite specimen with a constant displacement rate. The steel ball in the loading fixture allowed uniform compressive force dis-

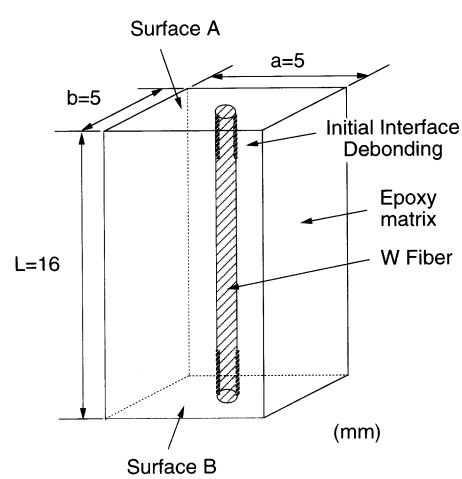

Fig. 1. Shape and dimensions of the specimen (mm).

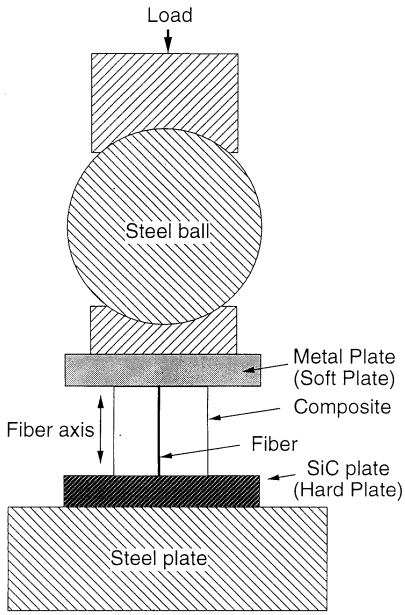

Fig. 2. Schematic drawing of loading system.

tributions at the contact surface between the specimen and the soft plate. The load was applied using an Instron testing machine (maximum capacity 500 kN, model 1726, Instron, USA) with a constant crosshead displacement rate of 0.5 mm min^{-1} at the room temperature (297 K) in air. The applied compressive load ranged from 0.13 to 1 kN corresponding to a compressive stress ranged from 5 to 35 MPa. It should be noted that this maximum applied stress was below the compressive yield stress of epoxy matrix (= 50 MPa [21]). When the applied load reached a set point, the load was kept for 15 s, and then, unloaded at a rate of 0.5 mm min^{-1}. The load during the period of 15 s was constant and no influence of the loading system on the test procedure could be assumed.

2.3. Direct observation of interface sliding behavior

During the loading/unloading process, the side of specimen was illuminated by a white light and the reflected light was monitored by a video-microscope to allow the determination of an interface debonding length. This technique has been successfully applied for observation of interface debonding/sliding behaviors in SiC fiber-reinforced PMMA [22] and SiC fiber-reinforced glass matrix composites [10]. The images from the video-microscope were first stored to a VTR and were then processed using a public domain 'NIH-Image' software to enhance the contrast.

For selected specimens, loading was interrupted at a set-point and then followed by unloading. The interface debonding length was determined by the transmitted cross-polarized light under a conventional optical microscope. In this case, the direction of the incident light was perpendicular to the fiber axis of the tested specimen.

2.4. Fiber protrusion behavior

The fiber protrusion length at the aluminum plate side was measured by scanning electron microscope (SEM) and scanning laser optical microscope (SLOM: LM-21, Lasertech, Yokohama, Japan). The length of protruded fiber from the matrix was also measured by SLOM. The nominal resolution of scanning laser optical microscope was less than 0.1 μm.

3. Experimental results and discussion

3.1. Interface debonding and sliding process

Fig. 3 shows a typical example of progress of interface debonding behavior with applied stress, σ^a, obtained by direct observation. The arrows in the photographs indicate the observed interface debond front during the test. The debond interface is clearly distinguished from the change of the reflected light from the interface. The interface debonding from an initial debond tip proceeds when the applied stress, σ^a, reaches a critical stress, σ_c^a. Here, the applied stress, σ^a, (compression) is defined as the applied force, F^a, divided by the transverse cross-sectional area of composite specimen. In Fig. 3 the interface sliding from the initial sliding front starts when the applied stress, σ^a, reaches ≈ 15 MPa ($= \sigma_c^a$), then the interface sliding length increases with the increase of the applied stress.

The interface sliding proceeds spontaneously with a typical unit debond length of ≈ 500 μm ($\approx 2R_f$: R_f is the radius of fiber), as schematically illustrated in Fig. 4. This debonding process is observed in all the applied loading conditions. The interface debonding progress from the hard plate (SiC plate) side is not observed under the present experimental conditions. During the progress of interface debonding, two states are expected in the debond interface; the stick condition and the slide condition [23] because radial compressive stress is acting at the sliding interface[1].

Just after the progress of spontaneous unit debonding, the interface shear stress remains below its critical value for onset of the sliding and therefore the interface

[1] The thermal expansion coefficient of the W fiber, α_f, is 4.6×10^{-6} K^{-1} [19] and that of the epoxy matrix, α_m is 60×10^{-6} K^{-1} [18]; i.e., $\alpha_f < \alpha_m$. Therefore, before loading, a compressive radial clamping stress is acting at the interface. Loading condition of the experiment satisfies the frictional interface condition, $-(\sigma^r + \sigma^P) < 0$, where σ^r and σ^P are the radial compressive clamping stresses due to thermal expansion mismatch and Poisson's effect, respectively. The interface condition during the compression test has been discussed in reference [15].

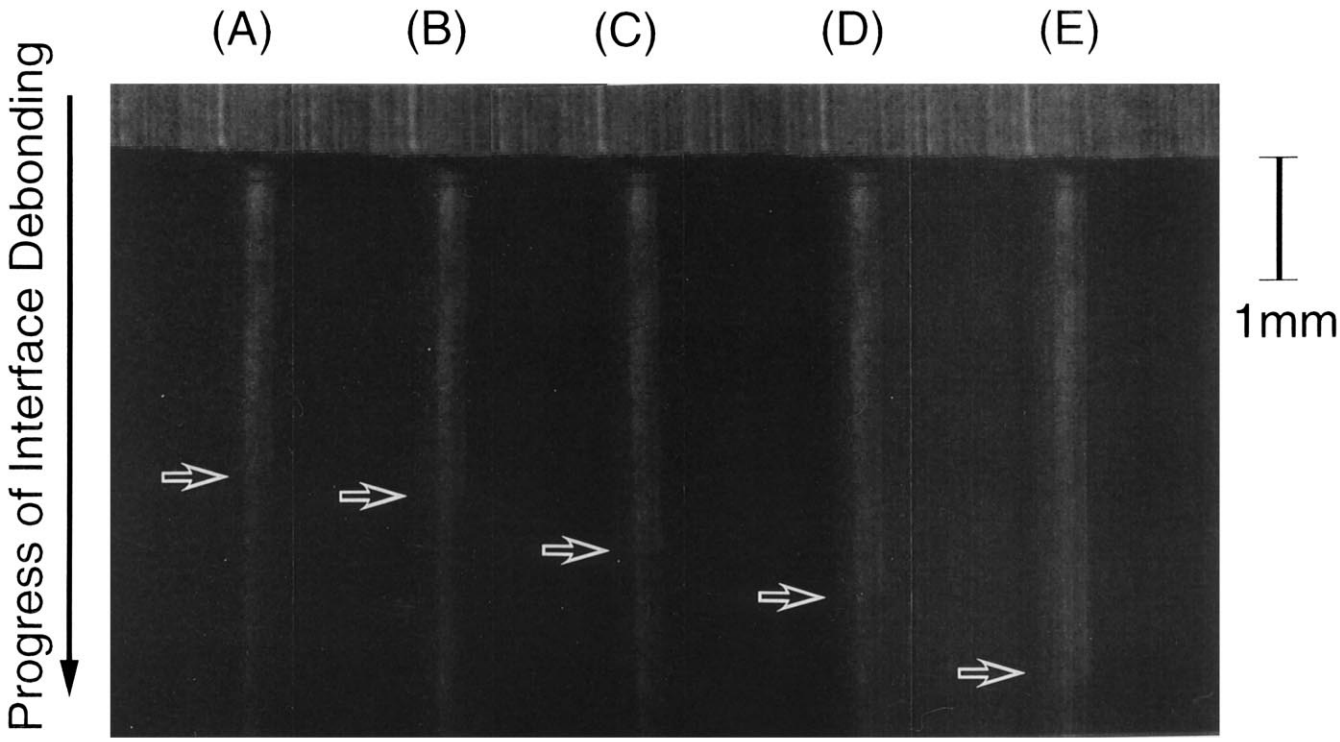

Fig. 3. A typical example of the progress of interface sliding during the protrusion test (arrows indicated debond tip).

remains a stick state. The stick condition at the interface locks relative sliding between fiber and matrix, hence, the shear stress at the debond tip could not increase sufficiently to overcome debonding although the applied stress, σ^a, increases. Once the stick state is overcome, the interface slides and correspondingly the debond tip shear stress increases. When the debond tip shear stress rises sufficiently large (i.e. critical value), next debonding proceeds spontaneously. This process is repeated during the protrusion test and therefore causes the spontaneous interface debonding process.

Just before the progress of a spontaneous debonding, all the debonded interface slides and thus the debonded length is assumed to be equal to the interface sliding length I_s. Hereafter, the interface sliding length and the corresponding load are defined in this condition (Fig. 4). Fig. 5 is the plots of interface sliding length, l_s, versus applied stress, σ^a, for two different initial debond length specimens; $l_s^0 = 1.5$ and 2.9 mm. At the beginning of compressive loading, the sliding length does not increase until the critical applied stress, σ_c^a, is reached. Because the progress of sliding must overcome frictional resistance of the initial debonding area. The critical stresses are $\sigma_c^a = 6.8$ and 15 MPa for the initial debond length $l_d^0 = 1.5$ and 2.9 mm, respectively. The critical stress, σ_c^a, depends on the initial debond length and a larger critical stress is required for a larger initial debond length.

After the applied stress increases above the critical stress, σ_c^a, the interface sliding length increases linearly with the increase of the applied stress. However, the increase rate, defined as $dl_s/d\sigma^a$, gradually increases above $\sigma^a = 25$ MPa. According to the shear lag analysis with a constant shear stress, the relation between applied stress and interface shear sliding stress is given by Eq. (A-5)

$$l_s = \frac{(1-f)(E_f - E_m)R_f\sigma^a}{2\tau_s^F E_c} \tag{1}$$

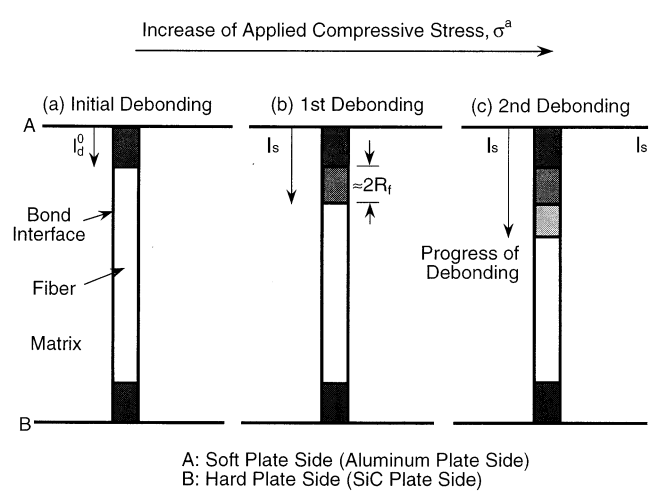

Fig. 4. Schematic drawing of progress of interface spontaneous debonding and definition of interface sliding length, l_s.

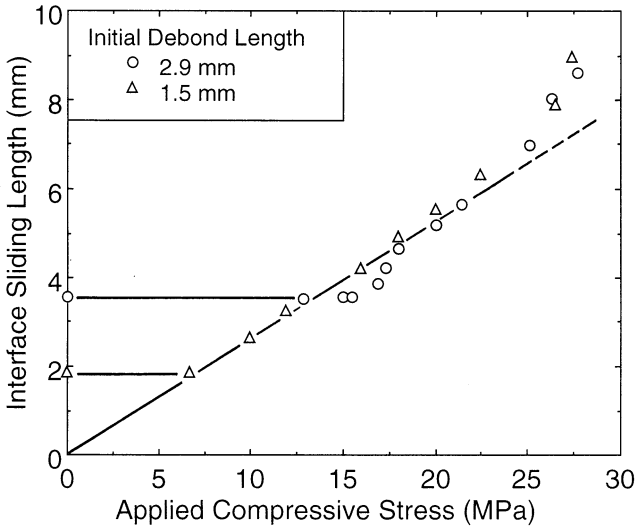

Fig. 5. Plots of interface sliding length, l_s, and applied stress, σ^a.

where f is the fiber volume fraction, E_f, E_m and E_c are Young's moduli of fiber, matrix and composite respectively, R_f is the fiber radius, σ^a is the applied stress and τ_s^F are interface shear stress at loading. This equation suggests that the interface sliding length, l_s, is linearly proportional to the applied stress, σ^a. The gradual increase of $dl_s/d\sigma^a$ above $\sigma^a = 25$ MPa could not be explained with this model. Prior to loading, interface keeps radial compression stress because of $\alpha_f < \sigma_m$. However, this radial compressive stress decreases with the increase of applied stress due to Poisson's effect because the greater compressive load makes the Poisson's effect greater [15]. Thus interface sliding at the debond interface becomes easier with the increase of applied compression axial stress, i.e. reducing interface shear frictional stress with the increase of σ^a. This result also indicates that the constant shear stress approach in the current composite is valid below $\sigma^a < 25$ MPa and also suggests existence of a critical maximum loading stress for a given material system.

3.2. Fiber protrusion behavior

Fig. 6 shows a typical example of SEM photograph of the protruded fiber. At $\sigma^a = 5$ MPa, the fiber protrusion behavior from the matrix is not observed. On the contrary, at $\sigma^a = 25$ MPa, the fiber is clearly protruded from the matrix. Detailed observation of the protruded fiber shows that the fiber is protruded ≈ 13 μm from the epoxy matrix and the rough W fiber surface is clearly observed.

A typical example of memory of fiber indentation in aluminum plate for $\sigma^a = 30$ MPa observed by SEM is shown in Fig. 7. The depth of the indentation means fiber protruded length during a loading stage because an elastic recovery of aluminum plate is assumed to be small. Fig. 8 is plots of the indentation depth, δ, and protruded fiber length after unloading, δ', as a function of square of the applied stress, $(\sigma^a)^2$. Both the lengths increase with the increase of applied stress. Both the relations below $(\sigma^a)^2 = \approx 650$ MPa^2 (i.e. $\sigma^a < 25$ MPa) are linear. In addition, the relation between δ and δ' for $\sigma^a < 25$ MPa follows:

$$\delta' \approx \frac{\delta}{2} \tag{2}$$

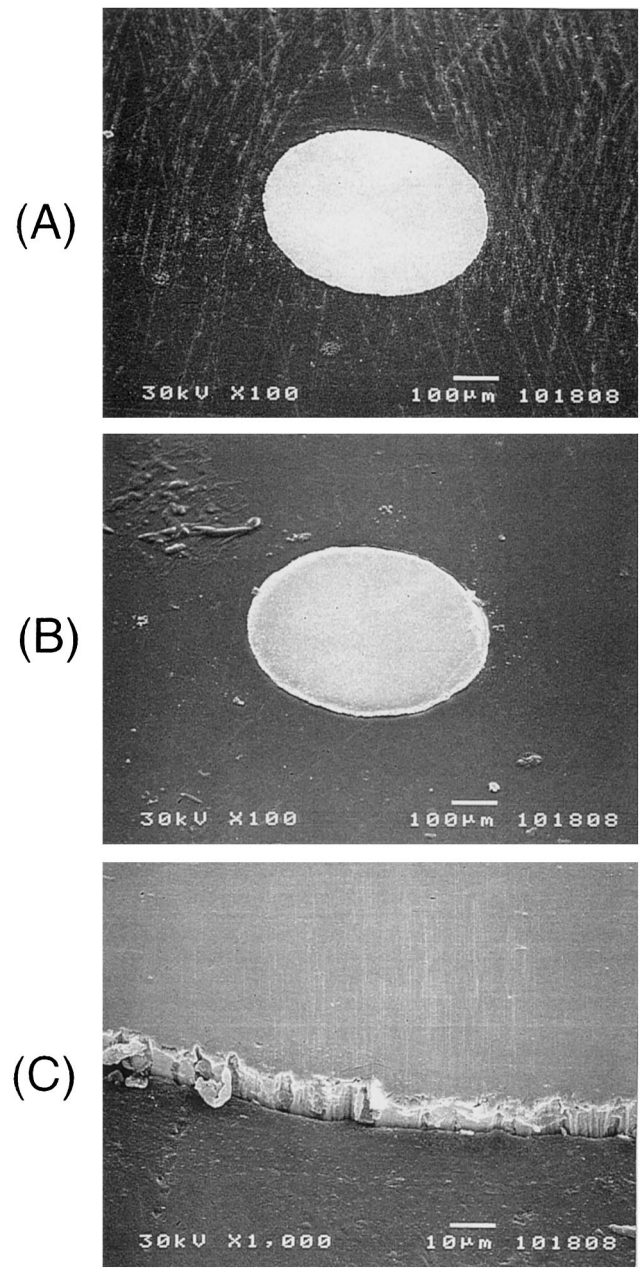

Fig. 6. Typical example of the appearance of protruded fiber with the applied stress, σ^a: (A) $\sigma^a = 5$ MPa; (B) $\sigma^a = 25$ MPa; and (C) $\sigma^a = 30$ MPa.

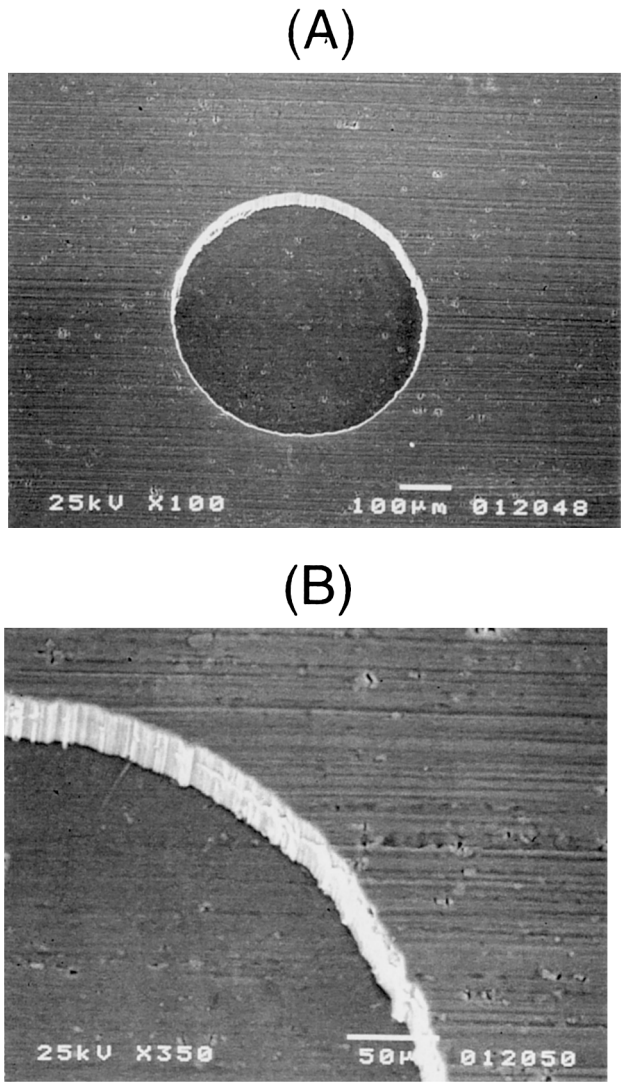

Fig. 7. A typical example of the memory of fiber indentation in aluminum plate ($\sigma^a = 30$ MPa).

The relation between the protruded lengths and interface shear sliding stresses is given by Eq. (A-25)

$$\delta' = \frac{\tau_s^R}{\tau_s^F + \tau_s^R}\,\delta \tag{3}$$

where τ_s^F and τ_s^R are the forward and reverse shear frictional stress, respectively. When $\tau_s^F \approx \tau_s^R$, the protrude fiber length after unloading, δ', becomes half of that at maximum compressive stress during loading, δ. The relation of Eq. (2) means that the forward and reverse interface shear sliding stresses are nearly equal ($\tau_s^F \approx \tau_s^R$) The relationship between δ and δ' does not coincide with Fig. 5, especially $\sigma^a > 25$ MPa; the protrusion length should increase because of the increase of $dl_s/d\sigma^a$. This behavior could be explained by experimental technique. With the increase of indentation depth of a fiber in the aluminum plate, the resistance for the indentation increases due to work hardening while shear frictional resistance decreases due to Poisson's effects [15]. Probably these two effects cancel the measured protrusion length at the metal plate. If the maximum protrusion length is limited, the protrusion length after complete unloading is also limited because reverse sliding at unloading stage occurs about half forward sliding length. However, within this study it is difficult to obtain quantitative treatment because the protrusion length is affected by various unknown experimental factors, such as frictional coefficient between metal plate and fiber, work hardening behavior of metal plate etc.

3.3. Interface shear sliding stress

The interface shear sliding stress of the composite is obtained from: (i) σ^a versus l_s ($\sigma^a - l_s$); (ii) σ^a versus δ ($\sigma^a - \delta$); and (iii) σ^a versus δ' ($\sigma^a - \delta'$). The obtained values from three different routes are compared. As discussed above, it is assumed that the interface forward and reverse sliding stresses are equal ($\tau_s^F \approx \tau_s^R$). To avoid Poisson's effect, the relations only for $\sigma^a < 25$ MPa are used for the prediction of interface shear sliding stress.

From Eq. (A-5), the interface shear sliding stress for a forward sliding, τ_s^F, is given by as a function of interface shear sliding length, l_s, and is given by

$$\tau_s^F = \frac{(1-f)(E_f - E_m)R_f\sigma^a}{2I_sE_c} \tag{4}$$

This equation suggests that the interface shear sliding stress is proportional to the applied stress. The

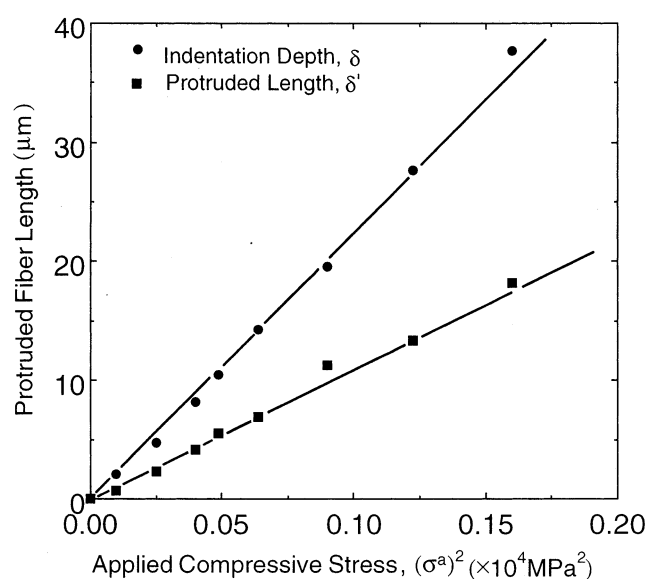

Fig. 8. Plots of fiber protrusion length at the maximum load, δ (obtained from the indentation depth) and after complete unloading, δ'.

interface shear sliding stress is obtained using the relation between σ^a and l_s (Fig. 5). The relation below $\sigma^a < 25$ MPa is linear and thus, the shear stress is obtained from this stress range. Least squares fitting of σ^a versus l_s relation yields $\tau_s = 29.9$ MPa.

The interface forward sliding stress is also obtained from a protruded length, δ, and applied stress, σ^a, relation as

$$\tau_s^F = \frac{(1-f)(E_f - E_m)^2 R_f (\sigma^a)^2}{4E_f E_m E_c \delta} \tag{5}$$

The interface shear sliding stress is given by the slope of protruded length versus square of the applied stress (Fig. 8). Least squares fitting of the relation gives interfacial shear sliding stress of 29.5 MPa.

On the other hand, the interface shear sliding stress after unloading, which includes both forward shear sliding and reverse shear sliding, is obtained from the relation between applied stress and protruded fiber length after complete unloading, δ'. The shear sliding stress is given by Eq. (A-23)

$$\tau_s^R = \frac{R_f E_f \tau_s^F \delta'}{(1+\alpha)\tau_s^F l_s^2 - R_f E_f \delta'} \tag{6}$$

Applying Eq. (6) and least squares fitting of the plots in Fig. 8 yields interfacial shear sliding stress of 27.8 MPa. This interfacial shear sliding stress is comparable with that obtained from the interface shear sliding length. This agreement suggests possibility of evaluation of constant interfacial shear sliding resistance using the protruded fiber length and applied stress. The critical applied stress depends on the composite and loading procedure, including properties of soft metal plate, and therefore care should be taken for the practical application of the protrusion method.

4. Conclusion

Direct observation of interface debonding/sliding behavior in W fiber-reinforced epoxy matrix composite during protrusion test has been studied. The interface shear sliding stress is obtained from three different routes using a constant shear stress approach. The following results are drawn.

(1) The onset of interface debonding from an initial debond tip proceeds above a critical applied stress, σ_c^a The critical stress needed to initiate debonding increases with the increase of the initial debond length l_d^0. Interface debonding proceeds spontaneously from interface at the soft metal side. The interface debond growth from hard plate side does not occur under the experimental condition.

(2) The relationships: (i) σ^a versus l_s ($\sigma^a - l_s$); (ii) σ^a versus δ ($\sigma^a - \delta$); and (iii) σ^a versus δ' ($\sigma^a - \delta'$). below the applied stress 25 MPa are well explained by the constant shear stress approach. Because, below the critical load, Poisson's effect can be ignored when the residue, clamping stress is large or the applied compressive load is low. For the constant interface shear stress approach, selection of the applied load range is important to avoid errors associate with loading process.

(3) Interface shear sliding stresses from three different routes (relationships (i) $\tau_s = 29.9$; (ii) $\tau_s = 29.5$; and (iii) $\tau_s = 27.8$ MPa) agree and this means possibility of obtaining interface shear slicing stress using a protrude fiber length from matrix. However, this agreement is limited only below a critical maximum applied stress because of Poisson's effect. Under the critical maximum applied stress, the constant shear frictional stress approach is valid for the evaluation.

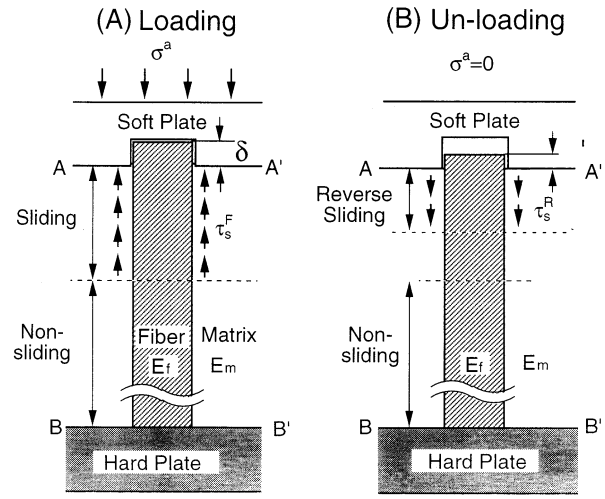

Fig. 9. Analytical model for the protrusion test.

Appendix A

The mathematical equations used to obtain the interfacial shear stresses are summarized here. The principle of the experimental technique is schematically shown in Fig. 9. The technique has two distinct regimes of behavior: (i) the composite has compressive force and interface will slide (forward sliding), and the reverse sliding at interface by the unloading of applied force. The mathematical equations to describe the interfacial shear sliding stress and protrusion length obtained here follows with a simple shear-lag analysis.

To simplify the analysis of experimental results, the shear sliding stress along the sliding interface is assumed to be constant, τ_s^F and τ_s^R. The thickness of the specimen, L, is assumed to be long enough compared with the sliding length, $l_s (L \gg l_s)$ and the effect of thermal expansion mismatch is neglected. A compressive stress, σ^a, is applied at the top end (A) of the composite via soft metal plate. The soft metal plate has a yield stress $\sigma_y = 0$. The other end (B) of the composite is located above a hard plate (assumed to be stiff plate).

The protruded length in the fiber at the surface, δ, is much smaller than that of the sliding length, $l_s(\delta \gg l_s)$. Further assumptions are similar to those used in the previous studies [11,12]. The stress, strain changes in fiber and matrix during loading and unloading stage are shown in Fig. 10.

A.1. Loading stage

The average fiber and matrix compressive stress, $\sigma_f(z)$, $\sigma_m(z)$. and interface shear forward sliding stress, τ_s^F, for $0 < z < l_s$, respectively, are given by

$$\sigma_f(z) = \sigma^a + \frac{2\tau_s^F}{R_f} \tag{A-1}$$

$$\sigma_m(z) = \sigma^a - \frac{2f\tau_s^F}{(1-f)R_f} z \tag{A-2}$$

The axial strains of fiber and matrix, $\varepsilon_f(z)$ and $\varepsilon_m(z)$, respectively, are

$$\varepsilon_f(z) = \frac{\sigma^a}{E_f} + \frac{2\tau_s^F}{R_f E_f} z \tag{A-3}$$

$$\varepsilon_m(z) = \frac{\sigma^a}{E_f} - \frac{2\alpha\tau_s^F}{R_f E_f} \tag{A-4}$$

where $\alpha = fE_f/(1-f)E_m$. The interface shear sliding length, l_s, is obtained assuming the fiber, matrix strains at the bond interface are the same ($\varepsilon_f(l_s) = \varepsilon_m(l_s)$) because of no shear stress is assumed above the debond front. Then, interface shear sliding stress is given as

$$l_s = \frac{(1-f)(E_f - E_m)R_f\sigma^a}{2\tau_s^F E_c} \tag{A-5}$$

where $E_c(= E_c = E_f f + E_m(1-f))$ is the longitudinal Young's modulus of the composite. The deformation of the fiber and matrix over the sliding length, l_s, respectively, are obtained integrating the strains (Eqs. (A-3) and (A-4)) over the range $z = 0$ to $z = l_s$,

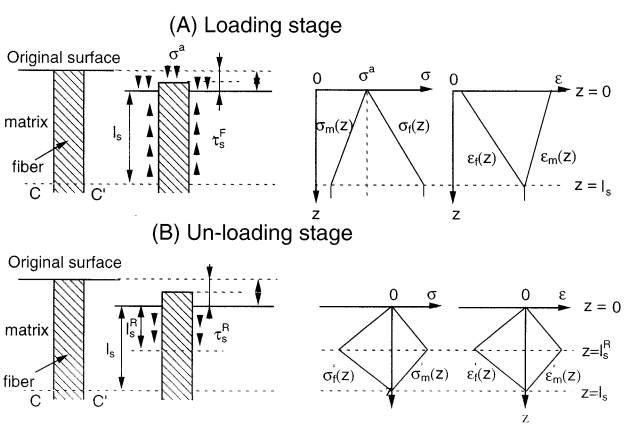

Fig. 10. Stress and strain distribution in fiber and matrix at loading stage (A) and unloading stage (B) during protrusion test.

$$\delta_f = \int_0^{l_s} \varepsilon_f(z)\,dz = \frac{\sigma^a l_s}{E_f} + \frac{\tau_s^F l_s^2}{R_f E_f} \tag{A-6}$$

$$\delta_m = \int_0^{l_s} \varepsilon_m(z)\,dz = \frac{\sigma^a l_s}{E_m} - \frac{\alpha\tau_s^F l_s^2}{R_f E_f} \tag{A-7}$$

The protruded fiber length, δ, under applied stress, σ^a, is obtained from differences of displacement between the fiber and matrix as

$$\delta = \delta_f - \delta_m = \frac{(1+\alpha)\tau_s^F l_s^2}{R_f E_f} \tag{A-8}$$

Substituting Eq. (A-8) into Eq. (A-5), the interface shear forward sliding stress τ_s^F, is

$$\tau_s^F = \frac{(1-f)(E_f - E_m)^2 R_f (\sigma^a)^2}{4E_f E_m E_c \delta} \tag{A-9}$$

A.2. Unloading stage

During unloading stage, reverse shear sliding occurs from the surface and the maximum reverse sliding length is assumed to be l_s^R. The stress and strain distributions for $0 \le z \le l_s^F$ are the same with those of loading stage. On the other hand, the stress in the fiber and matrix during unloading stage for $l_s^R \le z \le l_s$, respectively, are

$$\sigma'_f(z) = \sigma^a - \frac{2\tau_s^R}{R_f} z \tag{A-10}$$

and

$$\sigma'_m(z) = \sigma^a + \frac{2f\tau_s^R}{(1-f)R_f} z \tag{A-11}$$

where τ_s^F is the reverse shear sliding stress. Associated fiber and matrix strains are

$$\varepsilon'_f(z) = \frac{\sigma^a}{E_f} - \frac{2\tau_s^R}{R_f E_f} z \tag{A-12}$$

and

$$\varepsilon'_m(z) = \frac{\sigma^a}{E_m} + \frac{2\alpha\tau_s^R}{R_f E_f} z \tag{A-13}$$

The stress and strain continuities at $z = l_s^R$, i.e. $\sigma_f(l_s^R) = \sigma'_f(l_s^R)$, $\sigma_m(l_s^R) = \sigma'_m(l_s^R)$, $\varepsilon_f(l_s^R) = \varepsilon'_f(l_s^R)$, $\varepsilon_m(l_s^R) = \varepsilon'_m(l_s^R)$, lead to this result

$$\sigma'_f(z) = \sigma'_f(l_s^R) + \frac{2\tau_s^F}{R_f}(z - l_s^R) = a^a - \frac{2(\tau_s^F + \tau_s^R)}{R_f} l_s^R + \frac{2\tau_s^F}{R_f}, \tag{A-14}$$

$$\sigma'_m(z) = \sigma^a + \frac{2f(\tau_s^F + \tau_s^R)}{(1-f)R_f} l_s^R - \frac{2f\tau_s^F}{(1-f)R_f} z \tag{A-15}$$

$$\varepsilon'_f(z) = \varepsilon'_f(l_s^R) + \frac{2\tau_s^F}{R_f E_f}(z - l_s^R) = \frac{\sigma^a}{E_f} - \frac{2(\tau_s^F + \tau_s^R)}{R_f E_f} l_s^R + \frac{2\tau_s^F}{R_f E_f} z, \tag{A-16}$$

$$\varepsilon'_{\mathrm{m}}(z)=\frac{\sigma^{\mathrm{a}}}{E_{\mathrm{m}}}+\frac{2\alpha(\tau_{\mathrm{s}}^{\mathrm{F}}+\tau_{\mathrm{s}}^{\mathrm{R}})}{R_{\mathrm{f}}E_{\mathrm{f}}}\,l_{\mathrm{s}}^{\mathrm{R}}-\frac{2\alpha\tau_{\mathrm{s}}^{\mathrm{F}}}{R_{\mathrm{f}}E_{\mathrm{f}}}\,z. \tag{A-17}$$

The stress and stress distributions after completely unloading are obtained from Eqs. (A-14), (A-15), (A-16) and (A-17) by setting $\sigma^{\mathrm{a}}=0$.

The protruded fiber length, δ', after completely unloading is given by integrating the strain difference between the fiber and matrix over the range $z=0$ to $z=l_{\mathrm{s}}$. The displacements of fiber and matrix, δ'_{f} and δ'_{m}, respectively, after unloading are

$$\begin{aligned}\delta'_{\mathrm{f}}&=\int_0^{l_{\mathrm{s}}^{\mathrm{R}}}\varepsilon'_{\mathrm{f}}(z)\,\mathrm{d}z+\int_{l_{\mathrm{s}}^{\mathrm{R}}}^{l_{\mathrm{s}}}\varepsilon'_{\mathrm{f}}(z)\,\mathrm{d}z\\&=\frac{1}{R_{\mathrm{f}}E_{\mathrm{f}}}\{(\tau_{\mathrm{s}}^{\mathrm{F}}+\tau_{\mathrm{s}}^{\mathrm{R}})(l_{\mathrm{s}}^{\mathrm{R}}-l_{\mathrm{s}})^2-\tau_{\mathrm{s}}^{\mathrm{R}}l_{\mathrm{s}}^{2\mathrm{R}}\},\end{aligned} \tag{A-18}$$

$$\begin{aligned}\delta'_{\mathrm{m}}&=\int_0^{l_{\mathrm{s}}^{\mathrm{R}}}\varepsilon'_{\mathrm{m}}(z)\,\mathrm{d}z+\int_{l_{\mathrm{s}}^{\mathrm{R}}}^{l_{\mathrm{s}}}\varepsilon'_{\mathrm{m}}(z)\,\mathrm{d}z\\&=-\frac{\alpha}{R_{\mathrm{f}}E_{\mathrm{f}}}\{(\tau_{\mathrm{s}}^{\mathrm{F}}+\tau_{\mathrm{s}}^{\mathrm{R}})(l_{\mathrm{s}}^{\mathrm{R}}-l_{\mathrm{s}})^2-\tau_{\mathrm{s}}^{\mathrm{R}}l_{\mathrm{s}}^2\}.\end{aligned} \tag{A-19}$$

From Eqs. (A-18) and (A-19), the displacements between fiber and matrix after unloading are

$$\delta'=\delta'_{\mathrm{f}}-\delta'_{\mathrm{m}}=\frac{1+\alpha}{R_{\mathrm{f}}E_{\mathrm{f}}}\{(\tau_{\mathrm{s}}^{\mathrm{F}}+\tau_{\mathrm{s}}^{\mathrm{R}})(l_{\mathrm{s}}^{\mathrm{R}}-l_{\mathrm{s}})^2-\tau_{\mathrm{s}}^{\mathrm{R}}l_{\mathrm{s}}^2\}. \tag{A-20}$$

Substituting $\sigma'_{\mathrm{f}}(l_{\mathrm{s}})=0$ at $\sigma^{\mathrm{a}}=0$, into Eq. (A-14), the reverse shear sliding length, $l_{\mathrm{s}}^{\mathrm{R}}$ is given by

$$l_{\mathrm{s}}^{\mathrm{R}}=\frac{\tau_{\mathrm{s}}^{\mathrm{F}}}{\tau_{\mathrm{s}}^{\mathrm{F}}+\tau_{\mathrm{s}}^{\mathrm{R}}}\,l_{\mathrm{s}} \tag{A-21}$$

Substituting Eq. (A-21) into Eq. (A-20), δ' is given by

$$\delta'=\frac{(1+\alpha)\tau_{\mathrm{s}}^{\mathrm{F}}\tau_{\mathrm{s}}^{\mathrm{R}}l_{\mathrm{s}}^2}{R_{\mathrm{f}}E_{\mathrm{f}}(\tau_{\mathrm{s}}^{\mathrm{F}}+\tau_{\mathrm{s}}^{\mathrm{R}})} \tag{A-22}$$

The reverse interface shear sliding stress is obtained from Eq. (A-22) as

$$\tau_{\mathrm{s}}^{\mathrm{R}}=\frac{R_{\mathrm{f}}E_{\mathrm{f}}\tau_{\mathrm{s}}^{\mathrm{F}}\delta'}{(1+\alpha)\tau_{\mathrm{s}}^{\mathrm{F}}l_{\mathrm{s}}^2-R_{\mathrm{f}}E_{\mathrm{f}}\delta'} \tag{A-23}$$

Further, substituting Eq. (A-5) into Eq. (A-23) yields

$$\tau_{\mathrm{s}}^{\mathrm{R}}=\frac{\delta'}{\delta-\delta'}\,\tau_{\mathrm{s}}^{\mathrm{F}} \tag{A-24}$$

From Eq. (A-24),

$$\delta'=\frac{\tau_{\mathrm{s}}^{\mathrm{F}}}{\tau_{\mathrm{s}}^{\mathrm{F}}+\tau_{\mathrm{s}}^{\mathrm{R}}}\,\delta \tag{A-25}$$

References

[1] D.B. Marshall, J. Am. Ceram. Soc. 67 (1984) 259–260.
[2] D.B. Marshall, W.C. Oliver, J. Am. Ceram. Soc. 70 (1987) 542–548.
[3] J.D. Bright, D.K. Shetty, C.W. Griffin, S.Y. Limaye, J. Am. Ceram. Soc. 72 (1989) 1891–1898.
[4] D.K. Shetty, J. Am. Ceram. Soc. 71 (1988) 107–109.
[5] K. Honda, Y. Kagawa, Acta Metall. Mater. 43 (1995) 1477–1487.
[6] D.H. Grande, J.F. Marshall, J. Mater. Sci. 23 (1) (1988) 311–328.
[7] T.J. Mackin, F.W. Zok, J. Am. Ceram. Soc. 75 (1992) 3169–3171.
[8] J.V. Bright, D.K. Shetty, C.W. Griffin, S.Y. Limaye, J. Am. Ceram. Soc. 72 (1989) 1891–1898.
[9] M.C. Watson, T.W. Cryne, Acta Metall. Mater. 40 (1992) 131–139.
[10] K. Honda, Y. Kagawa, Acta Metall. Mater. 44 (1996) 3267–3277.
[11] Y. Kagawa, K. Honda, Ceram. Eng. Sci. Proc. 12 (7–8) (1991) 1127–1137.
[12] K. Honda, Y. Kagawa, J. Jpn. Inst. Metall. 56 (1992) 1360–1370.
[13] N. Shafty, D.G. Brandon, M. Terasaki, Euro-Ceram. 3 (1989) 453–457.
[14] T. Johansson, A. Brückner-Foit, D. Brandon, N. Shafry, Proc. High-Temperature Ceramic-Matrix Composites I (Ceram. Trans., vol. 51) (1995) 305–310.
[15] C.H. Hsueh, Acta Metall. Mater. 41 (1995) 3585–3593.
[16] C.H. Hsueh, J. Composite Mater. 28 (1994) 638–655.
[17] Y. Kagawa, H. Iba, T. Chang, M. Tanaka, Acta Mater. 46 (1998) 265–271.
[18] H. Iba, Y. Kagawa, Philos. Mag. B 78 (1998) 37–52.
[19] T.H. Courtney, Mechanical Behavior of Materials, McGraw-Hill, New York, 1990.
[20] K. Honda, Y. Kagawa, J. Jpn. Inst. Metall. 56 (1992) 481–489.
[21] H. Iba, T. Chang, Y. Kagawa, to be contributed.
[22] K. Goto, Y. Kagawa, K. Nojima, H. Iba, Mater. Sci. Eng. A212 (1996) 69–74.
[23] Y.-F. Liu, Y. Kagawa, Mater. Sci. Eng. A212 (1996) 75–86.